PAPER

Check for updates

An indacenodithiophene-based semiconducting polymer with high ductility for stretchable organic electronics†

Yilin Li,[a] Wesley K. Tatum,[a] Jonathan W. Onorato, [ID][a] Sierra D. Barajas,[a] Yun Young Yang[a] and Christine K. Luscombe [ID] *[a,b,c]

An alkyl-substituted indacenodithiophene-based donor–acceptor π-conjugated polymer (**PIDTBPD**) with low stiffness and high ductility is reported. The polymer was synthesized after DFT calculations predicted that it would have a kinked backbone conformation while showing strong intramolecular charge transfer (ICT), suggestive of the fact that it would be beneficial to the polymer's elasticity and charge mobility. Atom-efficient direct arylation polymerization (DArP) was exploited to synthesize the polymer. Mechanical studies indicate that **PIDTBPD** has relatively rapid stress-relaxation properties, which lead to a low elastic modulus of 200 MPa and high crack-onset strain of *ca.* 40% (lower limit). A moderate charge carrier mobility of 2×10^{-3} cm^2 V^{-1} s^{-1} with a current on/off ratio of 2.5×10^6 was obtained from the fabricated OFETs. Further experiments were performed to elucidate the structural aspects of this polymer: UV-Vis and PL spectra suggest that minimal conformational change occurs in the polymer between its diluted solution and thin film states; DSC measurements indicate that the polymer's T_g is below −20 °C, allowing it to be in a rubbery state at room temperature; and XRD studies support this observation suggesting that the polymer is mostly amorphous at room temperature.

Introduction

In the past few decades, organic semiconductors have been the focus of both scientific research and industrial applications because of their interesting (opto)electronic properties and solution processability. They have been successfully employed and extensively studied in the fields of organic photovoltaics (OPVs),[1] organic field-effect transistors (OFETs),[2] organic light-emitting diodes (OLEDs)[3] and organic thermoelectrics (OTEs).[4] As their practical applications have extended into the health and life sciences areas (*e.g.*, electronic skins and artificial muscles), the mechanical compliance (*i.e.*, low stiffness and high ductility) has become increasingly important.[5,6] This in turn requires one to establish an understanding of the relationship between polymer structure and their mechanical properties as well as their (opto)electronic properties.[7]

Recently, a mechanical properties' study of a library of donor–acceptor π-conjugated polymers was reported.[8] The study revealed a relationship between the mechanical properties (*i.e.*, stiffness or elastic modulus (E_f) and ductility or crack-onset strain (CoS)), and polymer structure (*i.e.*, type of backbone and side chain, molecular weight and dispersity). Specifically, it was shown that among the total 51 polymers studied, only about 10 polymers exhibited more favorable mechanical properties than P3HT (*i.e.*, a lower stiffness and greater ductility than P3HT whose E_f = 1090 MPa and CoS = 9%) while most polymers were brittle and tended to fracture at low strains (CoS < 5%). Although this study suggested some promising design criteria for the polymers (*e.g.*, incorporation of phenyldithiophene into the polymer or the use of large branched solubilizing side chains), considering that the number of π-conjugated polymers is still limited, it is desirable to develop alternative polymers with good mechanical properties while still showing decent (opto)electronic properties.

Among the nearly limitless number of π-conjugated structures for organic semiconductors, alkyl-substituted indacenodithiophene (**IDT**) has recently been recognized as a promising building block because of its planar backbone that facilitates π-electron delocalization and charge transport. Because of this, IDT-based small molecules, oligomers and polymers have made significant contributions to the advancement of organic

[a]Department of Materials Science and Engineering, University of Washington, Seattle, WA 98195, USA. E-mail: luscombe@uw.edu
[b]Department of Chemistry, University of Washington, Seattle, WA 98195, USA
[c]Molecular Engineering & Sciences Institute, University of Washington, WA 98195, USA

†Electronic supplementary information (ESI) available: Experimental, supplementary figures and tables, and compound characterization data. See DOI: 10.1039/c7py00435d

electronics such as OPVs[9–11] and OFETs.[12–14] Studies on an IDT-based polymer (IDTBT) discovered by the McCulloch group,[12] suggested that high mobility can be achieved without having long-range order.[15,16] Therefore, developing IDT-based polymers could be a promising approach to optimize both mechanical and (opto)electronic properties.

To date, most donor–acceptor π-conjugated polymers are synthesized using traditional Stille and Suzuki cross-coupling reactions.[17,18] However, these approaches show disadvantages such as the necessity of pre-functionalization of monomers (*e.g.*, by synthesizing arylstannanes or arylboron derivatives), the use of flammable and unstable organolithium reagents, and the formation of toxic by-products such as organotin compounds particularly for Stille coupling. To synthesize donor–acceptor π-conjugated polymers *via* an economically efficient and a more environmentally friendly approach, special attention has been paid to direct arylation polymerization (DArP), in which aryl carbon–hydrogen (C–H) bonds are catalytically activated.[19,20]

In this report, we present an IDT-based donor–acceptor π-conjugated polymer, **PIDTBPD**, whose chemical structure is shown in Fig. 1. The discovery of this polymer originated from our search for polymers with potentially high elasticity and charge mobility through density functional theory (DFT) calculations. As predicted, the synthesized polymer *via* DArP exhibited low stiffness, high ductility in addition to moderate charge mobility. Detailed structure–property relationships of this polymer were investigated using ultraviolet-visible (UV-Vis) and photoluminescence (PL) spectroscopies, differential scanning calorimetry (DSC), and X-ray diffraction (XRD) measurements indicating that **PIDTBPD** is a potentially useful material in stretchable organic electronics.

Results and discussion

Computational results

Theoretical calculations using DFT have long been considered a powerful tool to reveal the nature of various properties (*e.g.*, photovoltaic properties and charge mobility) of organic semiconductors. McCormick *et al.* previously suggested that the use of four repeating units (*n* = 4) for computing donor–acceptor π-conjugated polymers can accurately represent the saturation length of the polymer, at which the (opto)electronic properties exhibit minimal change by adding more repeating units.[21] To begin our studies, a series of IDT-based donor–acceptor π-conjugated structures (*n* = 4) were modeled, and one specific
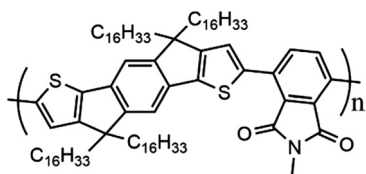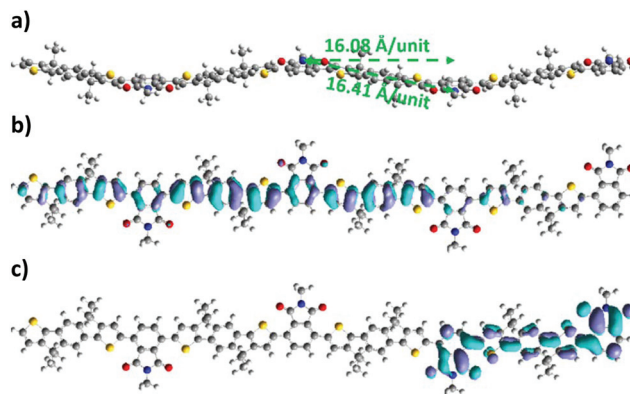

Fig. 2   (a) Kinked backbone conformation of **PIDTBPD** (*n* = 4); and its charge distribution in the (b) HOMO and (c) LUMO.

polymer, **PIDTBPD**, comprised of benzopyrrolodione (**BPD**) as an acceptor unit connected to **IDT**, drew our attention. As depicted in Fig. 2a, it shows a kinked backbone conformation induced by a twisted and bent conjugation (discussed later, Fig. 3a), which implies a potential structural elongation of 2% (= 16.41 Å/16.08 Å − 1) when the structure is stretched to a linear state. Moreover, this kinked backbone conformation would disrupt the alkyl side chain packing of the molecule to reduce the intermolecular interaction, thereby reducing the barrier to chain motion, and resulting in a lower elastic modulus. The localized charge distribution of the polymer in the highest occupied molecular orbital (HOMO) and the lowest unoccupied orbital (LUMO) shown in Fig. 2b and c, respectively, indicates that the polymer would demonstrate strong intramolecular charge transfer (ICT) (discussed later, Fig. 3b). The unique structural and electronic features would be beneficial to the polymer's elasticity and charge mobility.

After the preliminary investigations, detailed DFT calculations were performed on the monomer (*n* = 1) and oligomers (*n* = 2–7) of **PIDTBPD** to investigate the reason for the kinked backbone conformation. As shown in Fig. 3a, a dihedral angle of 27.5° between the **IDT** and **BPD** units ($\theta_{\text{IDT–BPD}}$) were found in the oligomers (*n* = 2–7) but not in the monomer (*n* = 1 with $\theta_{\text{IDT–BPD}}$ = 0°) in their optimal ground state geometries. The dihedral angle comes from a twisted and bent conjugation with the latter contributing to the kinked feature of the backbone conformation. Further investigations into these ground state geometries indicated that the kinked backbone is most likely caused by steric hindrance between the **IDT** and **BPD** units. Specifically, comparisons were made between the monomer and the oligomers by looking at three atomic distances in **IDT** and **BPD** as shown in Fig. 3b: the length of the σ-bond ($d_{\text{IDT–BPD}}$), the distance between two H atoms ($d_{\text{H–H}}$), and the distance between the S and O atoms ($d_{\text{S–O}}$). Calculations for the monomer show that the optimal distances for coplanarity are 1.47 Å, 1.93 Å and 2.76 Å for $d_{\text{IDT–BPD}}$, $d_{\text{H–H}}$ and $d_{\text{S–O}}$, respectively. Since $d_{\text{IDT–BPD}}$ remains unchanged (black solid line) with increasing *n*, $d_{\text{H–H}}$ and $d_{\text{S–O}}$ need to be shortened to 1.88 Å (blue dashed line) and 2.60 Å (red dashed line), respectively, to
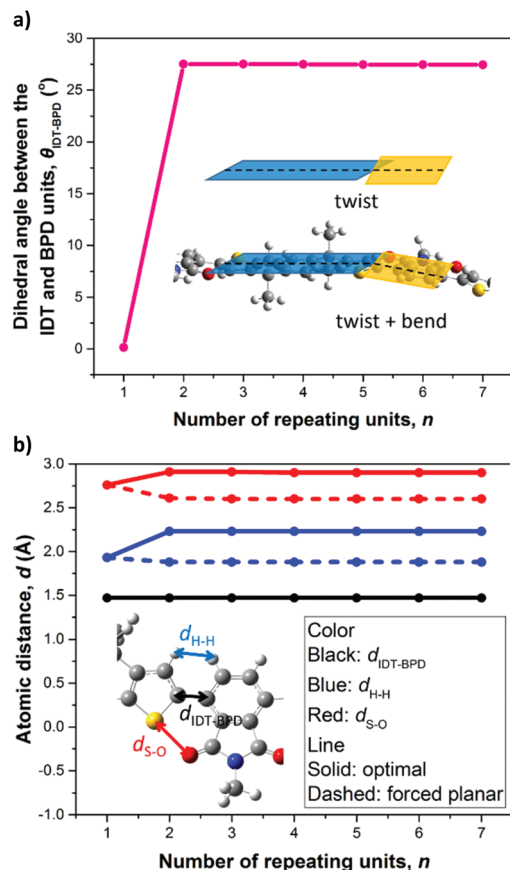

Fig. 1   Chemical structure of **PIDTBPD**.

Fig. 3 (a) Dihedral angle between the **IDT** and **BPD** units for the structures with different number of repeating units; and (b) atomic distance between specified atoms for the structures with different number of repeating units under the conditions of optimal and forced planar conformation.

maintain coplanarity in the oligomers (this was achieved by forcing the $\theta_{IDT-BPD}$ to 0°). These distances, which are shorter than what is required for the monomer, will cause greater steric hindrance in the oligomers. Therefore, coplanarity between the **IDT** and **BPD** units must be sacrificed to reduce steric hindrance resulting in the increase in d_{H-H} and d_{S-O} to 2.23 Å (blue solid line) and 2.90 Å (red solid line), respectively. The steric hindrance between the **IDT** and **BPD** units makes the polymer adopt a kinked backbone conformation instead of a linear one, which is expected to enhance the polymer's elasticity.

Calculations on the charge distribution of the structures with different repeating units in the HOMO and LUMO were also performed. The charge distribution percentages on each **IDT** and **BPD** unit for the monomer ($n = 1$) and oligomers ($n = 2-7$) are plotted in Fig. 4. Fig. 4a shows that the HOMO is primarily localized on **IDT** and minimally on **BPD**. This observation confirms that **IDT** is electron-rich, while **BPD** is electron-deficient. Furthermore, as n increases, charges are mostly on the second through fifth **IDT** unit, showing that the HOMO is moderately localized. Fig. 4b shows that charges are mostly on the **BPD** unit for the LUMO, which become highly localized on the last three units with increasing n. The trend observed for
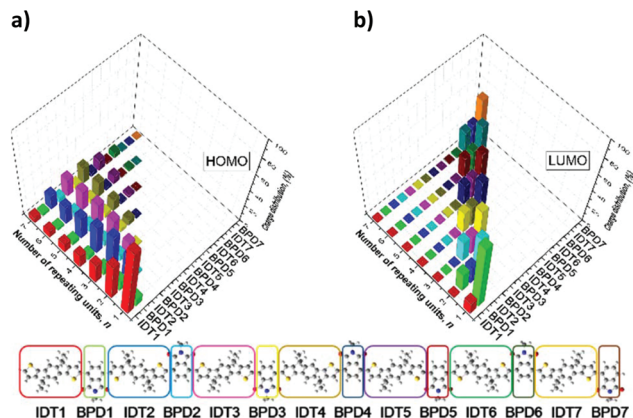

Fig. 4 Charge distribution on the **IDT** and **BPD** units of structures with differing number of repeating units ($n = 1-7$) in the (a) HOMO and (b) LUMO.

the calculated charge distribution (Table S1 in ESI†) suggests that the extended structures (*i.e.*, the structures of **PIDTBPD**) would also exhibit localized HOMO and LUMO and strong ICT would also occur across the entire backbone. The localized HOMO and LUMO can be ascribed to the insufficient p-orbital overlap due to the lack of structural coplanarity.[22,23] The strong ICT implies that the polymer may have efficient intramolecular charge transport. Overall, DFT calculations show that **PIDTBPD** is expected to have high elasticity and charge mobility.

Polymer synthesis

The synthesis of **PIDTBPD** is shown in Scheme 1. The monomer **IDT** was synthesized using modified literature procedures.[12,24,25] No particular changes were made to the syntheses of **1–5**, while changes were made to reactions (vi) and (vii) for the syntheses of **6** and then **IDT**, especially in their purification procedures. In synthesizing **6**, the exactly same procedure was used by Zhang *et al.*[12] and Wang *et al.*,[24] but the former reported the formation of a pale yellow solid while the latter reported a brown solid after washing the residue using water and acetone. A modified purification procedure was used by Cai *et al.*,[25] in which a pale yellow solid was obtained after column chromatography but without the water and acetone washing steps. In our efforts to synthesize **6**, it was found that the brown and yellow solids were in fact impure **6**. After dissolving the brown solid in acetone and filtering, a large portion of acetone-insoluble impurities could be removed. Recrystallization followed by further purification using column chromatography afforded highly pure **6** (Table S2 in ESI†) as an off-white solid soluble in chloroform.

Similarly, for the synthesis of **IDT**, we found that the one-step purification by column chromatography was insufficient to obtain the pure compound as described in literature,[12,24,25] because the side product, 1-hexadecene, produced from the elimination reaction between 1-bromohexadecane and sodium *tert*-butoxide, showed a similar polarity to **IDT**. Recrystallizing crude **IDT** in petroleum ether before column chromatography
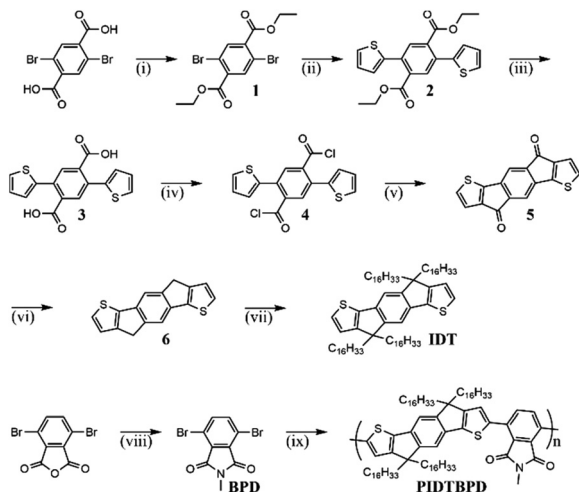
Scheme 1 Synthetic route of **PIDTBPD**. Reagents and conditions: (i) EtOH, conc. H_2SO_4, reflux, 16 h; (ii) 2-(tributylstannyl)thiophene, Pd $(PPh_3)_4$, toluene, N_2, reflux, 16 h; (iii) NaOH, MeOH/H_2O (1:1), reflux, 16 h; (iv) oxalyl chloride, DMF, DCM, N_2, RT, 2 h; (v) AlCl$_3$, DCM, N_2, RT, 16 h; (vi) KOH, diethylene glycol, a) 110 °C, 1 h, b) 180 °C, 4 h; (vii) 1-bro-mohexadecane, sodium *tert*-butoxide, toluene/DMSO (1:1), 80 °C, 1 h, 85 °C, 16 h; (viii) a) methylamine, THF, N_2, 0 °C → RT, 16 h, b) NaOAc, Ac$_2$O, 90 °C, 16 h; (ix) **IDT**, Pd$_2$(dba)$_3$, P(*o*-anisyl)$_3$, Cs$_2$CO$_3$, PivOH, *o*-xylene, 100 °C, 16 h.

Fig. 5 Aromatic regions in (a) ^1H and (b) ^{13}C NMR spectra of **PIDTBPD**.

Fig. 6 Photographs of (a) **PIDTBPD**, (b) P3HT, (c) PTB7, (d) IDTBT solids; a piece of **PIDTBPD** solid (e) before, (f) during and (g) after compression between two glass slides; and (h) a free standing compressed **PIDTBPD** solid.

removed most of the 1-hexadecene, and further recrystalliza-tion after column chromatography afforded highly pure **IDT** (Table S2 in ESI†) as an off-white solid. Further reaction of **IDT** with **BPD** through DArP[26] yielded the target polymer, **PIDTBPD**. The number- and weight-averaged molecular weights (M_n and M_w) of the polymer were 18 000 g mol^{-1} and 39 000 g mol^{-1}, respectively (Fig. S1 in ESI†), corresponding to a number-average degree of polymerization (DP$_n$) and a disper-sity (Đ) of 14 and 2.2, respectively.

NMR spectroscopy was used to verify the chemical structure of **PIDTBPD**. Fig. 5 shows the aromatic regions of its ^1H and ^{13}C NMR spectra. The two proton peaks in the ^1H NMR spec-trum and eleven individual carbon peaks in ^{13}C NMR are con-sistent with the number of proton and carbon environments in the polymer. The chemical shift at 7.39 ppm in the ^1H NMR spectrum is attributed to the protons on the 3-position of the thiophene, suggesting that C–H activation mostly occurred at the desirable 2-position of the thiophene during DArP support-ing the formation of a polymer with limited branching. According to the integration, the homocoupling (most likely between two **IDT** units)[27] percentage is about 0.26% (= 0.16/ 2.16–1/14), which is negligible. The NMR spectra suggest that the synthesized polymer has minimal structural defects.

The as-synthesized **PIDTBPD** was found to be soft and sticky and the solids are aggregated (Fig. 6a), while other π-conjugated polymers such as P3HT (Fig. 6b) and PTB7[28] (Fig. 6c) are rigid and powdery solids. IDTBT (M_n = 15 000 g mol^{-1} and M_w = 26 000 g mol^{-1}) was also synthesized *via* DArP in this study (Scheme S1 in ESI†) as a structural analog to **PIDTBPD** because it has the same structural backbone
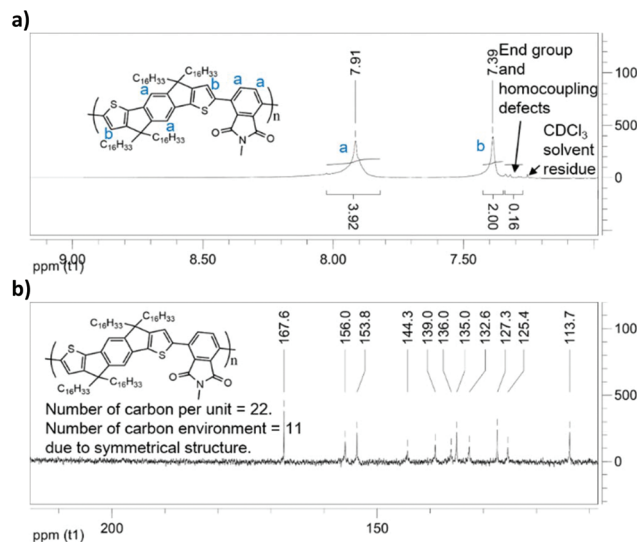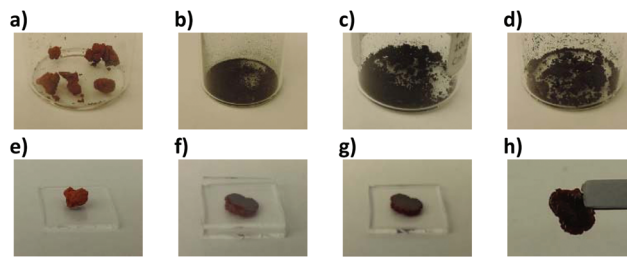
(*i.e.*, thiophene–phenylene–thiophene–phenylene) and length of alkyl side chain (*i.e.*, hexadecyl) as **PIDTBPD**. IDTBT exhibits a planar backbone conformation, allowing for a comparison of the effects of the non-planar backbone. It is noted that the synthesized IDTBT is also a rigid and powdery solid. The difference in solid form between **PIDTBPD** and IDTBT implies that the backbone conformation may play an important role in the stiffness and ductility of the polymer. The color of **PIDTBPD** is deep orange in general (Fig. 6a and e). However, after the polymer was compressed between two glass slides (Fig. 6f), both contact surfaces to the glass slides became dark (Fig. 6g and h). This observation indicates the possible piezo-chromic properties of the polymer, which may be attributed to a more ordered molecular arrangement.[29] These observations on the as-synthesized **PIDTBPD** were within our expectation from the DFT studies which led us to further investigate its mechanical and charge transport properties.

Mechanical properties

Measurements on the elastic modulus (E_f) and crack-onset strain (CoS) of the nanoscale-thick polymer films were per-
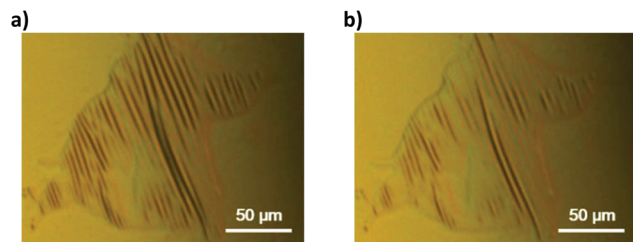
Fig. 7 Optical microscopy images of the buckling pattern observed in the polymer film (a) before and (b) after 5 minutes.

formed. The buckling-based metrology, originally observed by the Whitesides group,[30] further developed by the Stafford group,[31] and applied to semiconducting polymers by the Khang group,[32] was used to determine the elastic modulus (see ESI† for further details). To our surprise, after the stress was released to form the buckling pattern, the buckles gradually faded and eventually disappeared. Fig. 7 presents a region of the regular buckling pattern immediately after they were formed and after 5 minutes of leaving the film standing. Note that during the fading of the buckles, the buckling wavelength (periodic distance between two adjacent buckles) did not change. Hence, the fading of the buckles is due to the decrease in buckling height. Further crack-onset strain measurements showed that the polymer film did not delaminate from the polydimethylsiloxane (PDMS) substrate. Therefore, the faded buckling pattern indicates that the polymer exhibits significant stress-relaxation that occurs relatively rapidly. In spite of the fading buckling pattern, an approximate elastic modulus value of 200 MPa was determined through several distinct patterns prior to their fading (eqn (S1) in ESI†). The elastic modulus of **PIDTBPD** is one order of magnitude lower when compared against values observed for P3HT (E_f = 1000–1100 MPa)[32–34] and even lower than other donor–acceptor π-conjugated polymers (typically E_f > 300 MPa).[8] For stretchable organic electronics applications, a lower elastic modulus makes for a more broadly applicable material.

For a material to be useful in stretchable devices, it should have a high ductility in addition to a low elastic modulus. As such, crack-onset strain measurements were performed on the polymer films to determine their maximum elongation using a homemade strain stage (Fig. S2 in ESI†). In the measurements on a total of six polymer films, three were cracked while the others did not (Fig. S3 in ESI†). For the cracked polymer films, their crack-onset strains were estimated to be *ca.* 40%, which is near the extension limit of our homemade strain stage (41%). This value is significantly better than that of P3HT (CoS = 4.8%–9%)[8,33] and other donor–acceptor π-conjugated polymers (CoS < 15%).[8] It is important to note that the crack-onset strain measurements are not necessarily equivalent to the elongation at break, and often underestimate the value due to possible film defects during the preparation and imperfect adhesion to the substrate which result in the uneven distribution of stresses.[33] Therefore, it is reasonable to believe that the actual maximum elongation of **PIDTBPD** is higher than

40%. Regardless, these mechanical properties are very promising, and provide an encouraging argument for the potential use of the polymer as an active material in a stretchable organic electronic device with the added advantage of it being synthesized using DArP.

The mechanical properties of IDTBT were also measured and compared with those of **PIDTBPD** in order to further reveal the role of backbone conformation in the polymer's mechanical properties. The E_f of IDTBT is measured at 350 MPa with a well-structured non-fading buckling pattern (Fig. S4 in ESI†), while its CoS is measured at only *ca.* 3%. The role of a kinked backbone conformation in **PIDTBPD** is that it disrupts the alkyl side chain packing to reduce the intermolecular interaction. Therefore, **PIDTBPD** exhibits a lower E_f than IDTBT. The large difference in CoS between IDTBT and **PIDTBPD** is likely related to both the backbone conformation and the degree of packing of the alkyl side chains. The kinked backbone conformation of **PIDTBPD** not only introduces a potential 2% structural elongation from the straightening of the structure, but also reduces the interaction between side chains by disrupting the chain packing, which together contribute a CoS of up to *ca.* 40%.

Charge carrier mobility

Top-contact bottom-gate organic field-effect transistors (OFETs) were fabricated to measure the charge carrier mobility (μ) of **PIDTBPD** (see ESI† for further details). The relationship between the gate voltage (V_G) and the drain–source current (I_{DS}) as well as the device architecture is shown in Fig. 8. It was found that the polymer exhibited p-type behavior with a negative gate bias sweep from 0 to −100 V and a drain bias of −100 V. Under these conditions, the saturation regime of the square root of I_{DS} ($I_{DS}^{1/2}$) *vs.* V_G curve demonstrated a charge carrier mobility of 2×10^{-3} cm^2 V^{-1} s^{-1} ($\pm 1 \times 10^{-3}$ cm^2 V^{-1} s^{-1}) with a
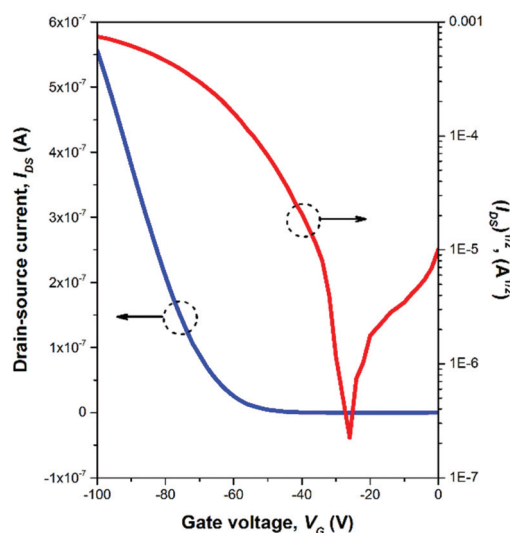

Fig. 8 Relationship between I_{DS} and V_G in a representative OFET. Inset picture: OFET architecture. S: source, D: drain, OTS: octadecyltrichlorosilane, In: indium.

current on/off ratio of 2.5×10^6 ($\pm 7 \times 10^5$) (eqn (S2) in ESI†). The devices were also tested for ambipolar properties by setting the drain bias to +100 V and sweeping the gate bias to +100 V from 0 V. They all displayed a low current flow under this n-type configuration. The mobility of **PIDTBPD** is higher than that of commonly spin-coated P3HT ($\mu = 4 \times 10^{-4}$–8.5×10^{-4} cm^2 V^{-1} s^{-1}, measured in our lab using the same device architecture as this report),[35] and ranks at the average of other stretchable π-conjugated polymers.[7] However, the mobility is significantly lower than that of its structural analog, IDTBT ($\mu = 1$–3.6 cm^2 V^{-1} s^{-1}),[12,15] which is primarily due to two factors. One is that our **PIDTBPD** synthesized has a lower molecular weight ($M_n = 18\,000$ g mol^{-1} with DP = 14) than the reported IDTBT ($M_n = 38\,000$ g mol^{-1} with DP = 29);[12] a relatively short backbone will cause inefficient charge transport in the polymer.[36,37] The other is that a top-gate bottom-contact OFET architecture was used for IDTBT and the device performance was optimized extensively,[12,15] while top-contact bottom-gate OFET architecture was used in our studies. The latter configuration cannot prevent the semiconducting layer from degrading through interactions with its surroundings (e.g., oxygen, water and light) thereby affecting the device performance.[38] Therefore, substantial improvement in the charge mobility of **PIDTBPD** is expected with optimization.

To further understand the structure–property relationship of **PIDTBPD**, the polymer was characterized for its thin film microstructure using UV-Vis and PL spectroscopies, DSC, and XRD.

Optoelectronic properties

The optoelectronic properties of **PIDTBPD** in dilute solution and thin film were studied using UV-Vis and PL spectroscopies. Fig. 9 depicts the absorption and emission spectra of **PIDTBPD** in dilute solution and thin film. The absorption spectra of **PIDTBPD** in solution and film are in the same wavelength region (450–550 nm) and with the same peak wave-

Fig. 9 UV-Vis and PL spectra of **PIDTBPD** in dilute solution and thin film.

length (ca. 515 nm) and the same is true of the emission spectra (550–650 nm and ca. 575 nm). This observation is quite different from typical conjugated polymers (e.g. P3HT, PTB7 and IDTBT), which show spectral shifted absorption and/or emission in thin films with respect to their solutions.[12,39,40] The spectral shift of typical conjugated polymers in films with respect to the solution is primarily attributed to the conformational change of the polymer in solution compared to the thin film. Specifically, planarization of the polymer backbone promotes the intramolecular p-orbital overlap and shifts the spectra to longer wavelengths.[41] The similarity in the spectra in solution and film suggest minimal conformational change in the polymer between the two conditions and that the polymer is flexible both in solution and in the thin film supporting our discussion on the kinked backbone conformation and helping to explain the observed mechanical properties.

The electronic transitions can also be known from the absorption and emission spectra of **PIDTBPD**. The 0-1 and 0-2 transitions are at 520 nm and 490 nm, respectively, while the 1-0 and 2-0 transitions are at 575 nm and 605 nm, respectively. The spectral symmetry with respect to the 0-0 transition at 550 nm is due to the equal shape of the ground and excited state potential wells according to the Franck–Condon principle.[42] Regarding the electrochemical properties of **PIDTBPD**, only the oxidation process was recorded during cyclic voltammetry (CV) because polymer degradation was observed during the reduction process, indicating that the polymer is p-type (Fig. S5 in ESI†), consistent with the OFET results. Its HOMO energy level (E_{HOMO}) with respect to ferrocene[43] ($E_{HOMO} = -4.8$ eV) is -5.58 eV while the LUMO energy level (E_{LUMO}) was estimated to be -3.32 eV using the optical band gap ($E_{g,opt}$) of 2.26 eV obtained from the Tauc plot[44] (Fig. S6 in ESI†).

Thermal properties

The differential scanning calorimetry (DSC) curve of **PIDTBPD** is depicted in Fig. 10. Three different thermal transitions (peaks labelled as 1, 2 and 3) were observed in all three heat–cool cycles that were performed. The endothermic transition in the heat cycle (peak 1) and the relative exothermic transition in the cool cycle (peak 3) are ascribed to the polymer's melting (T_m) and crystallization temperature (T_c), respectively. The T_m and T_c of **PIDTBPD** being below 0 °C is different from other typical π-conjugated polymers (e.g. P3HT[45] and PTB7[46]) that show T_m and T_c over 100 °C. The lower T_m and T_c of **PIDTBPD** than those of IDTBT (Fig. S7 in ESI†) suggests the effect of a kinked backbone conformation on the polymer's thermal properties, which disrupts the alkyl side chain packing to reduce the intermolecular interaction. It also indicates that the glass transition temperature (T_g) of **PIDTBPD** is below -20 °C, which implies that **PIDTBPD** is in a rubbery state at room temperature, which helps to explain its high deformability. Furthermore, **PIDTBPD** shows another endothermic transition around 160 °C; however, the relative exothermic transition is missing in the cooling cycle. The inset photographs show that when the polymer was heated to
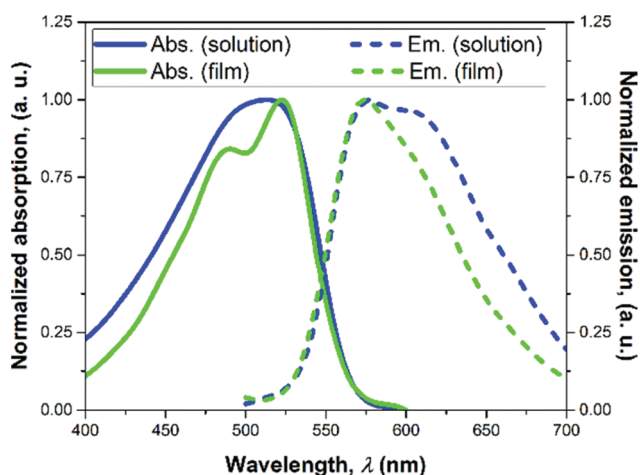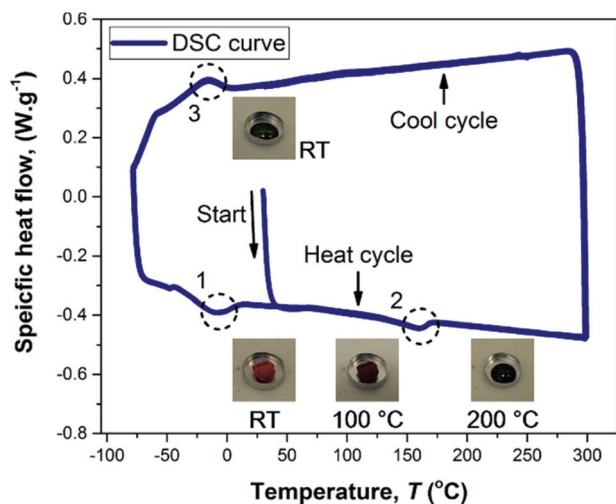
Fig. 10 DSC curve of **PIDTBPD**. Inset photographs: a polymer solid being heated on a hotplate from room temperature (RT) to 100 °C and to 200 °C and finally being cooled to room temperature.

Fig. 11 XRD patterns of **PIDTBPD** thin films before and after annealing at 200 °C.

200 °C, it experienced a transformation, changing from a deep orange solid to a droplet-like dark green solid, while cooling the polymer back to room temperature did not reverse this transformation. Though the nature of this transformation cannot be determined from the DSC curve, it can be speculated that the relative exothermic transition occurs at a slow rate and could occur across the whole cooling cycle. The presence of T_m and T_c peaks suggests that the polymer is not completely amorphous. The polymer was also investigated using thermal gravimetric analysis (TGA), which showed that in addition to a high thermal stability, that there was no moisture absorption or residual solvent contained in the polymer that could potentially act as a plasticizer, softening the material and affecting its mechanical properties (Fig. S8 in ESI†).

XRD results

Thin film XRD measurements were performed on **PIDTBPD** to investigate its thin film microstructure. Since the polymer showed a transformation (peak 2 and relative inset photographs in Fig. 10), the XRD data of the thin films before (orange line) and after annealing at 200 °C (gray line) were taken. The results are depicted in Fig. 11. For the as-cast film, the polymer showed a pronounced (100) diffraction peak at $2\theta = 3°$, arising from the interactions between the alkyl side chains, providing a d-spacing of 28.1 Å. In contrast, this peak disappeared for the annealed film, indicating that the alkyl side chains in the polymer became disordered. Therefore, the nature of the endothermic transition at peak 2 in the DSC curve of the polymer could be revealed as the disturbance of the alkyl side chain packing. Since **PIDTBPD** possesses four bulky alkyl side chains in its **IDT** unit, the rate for the alkyl side chains to return to an ordered packing pattern is expected to be slow, which is consistent with the observation that the polymer's lack of change in appearance after being cooled to room temperature. Furthermore, the (010) diffraction peaks at
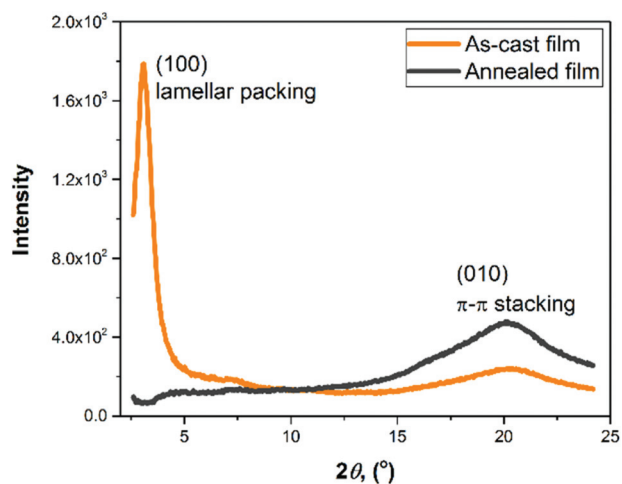
$2\theta = 20°$ were found for both the as-cast film and annealed film, which can be attributed to intermolecular π–π stacking with a d-spacing of 4.4 Å. Relatively broad peaks with low intensity indicate that the degree of crystallinity of **PIDTBPD** in the π–π stacking is low and the intermolecular interaction is weak, which leads to the polymer's high ductility.

Conclusions

In summary, during our search for polymers with high elasticity and charge mobility through theoretical calculations, an IDT-based donor–acceptor π-conjugated polymer (**PIDTBPD**) was discovered and expected to have a kinked backbone conformation while showing strong ICT. The polymer exhibits relatively rapid stress-relaxation properties with elastic modulus and crack-onset strain of 200 MPa and *ca.* 40% (lower limit), respectively. Its charge carrier mobility is 2×10^{-3} cm^2 V^{-1} s^{-1} with a current on/off ratio of 2.5×10^6. Structure–property relationship of the polymer was further analyzed by UV-Vis, PL, DSC and XRD. All the experiments suggested weak intermolecular interactions in the polymer molecules, which lead to a minimal conformation change of the polymer structure going from diluted solution to thin film, allowing it to be in a rubbery state and be mostly amorphous at room temperature. These results confirmed the computational studies, and allowed one to conclude that **PIDTBPD** is a promising candidate for stretchable organic electronics. This paper represents not just a simple introduction of a new polymer, but also the possibility to develop a series of similar polymers with potentially tuneable physical, mechanical and electronic properties by substituting with other alkyl side chains, using different acceptors or making a more kinked backbone conformation by adjusting the twist and bend between the donor and acceptor units, while still using the economically efficient and environmentally friendly DArP-based chemistry to synthesize the polymer.

References

1 K. A. Mazzio and C. K. Luscombe, *Chem. Soc. Rev.*, 2015, **44**, 78–90.

2 L. Torsi, M. Magliulo, K. Manoli and G. Palazzo, *Chem. Soc. Rev.*, 2013, **42**, 8612–8628.

3 B. Geffroy, P. L. Roy and C. Prat, *Polym. Int.*, 2006, **55**, 572–582.

4 B. Russ, A. Glaudell, J. J. Urban, M. L. Chabinyc and R. A. Segalman, *Nat. Rev. Mater.*, 2016, **1**, 16050.

5 G. Schwartz, B. C. Tee, J. Mei, A. L. Appleton, D. H. Kim, H. Wang and Z. Bao, *Nat. Commun.*, 2013, **4**, 1859.

6 T. Yokota, P. Zalar, M. Kaltenbrunner, H. Jinno, N. Matsuhisa, H. Kitanosako, Y. Tachibana, W. Yukita, M. Koizumi and T. Someya, *Sci. Adv.*, 2016, **2**, e1501856.

7 J. Onorato, V. Pakhnyuk and C. K. Luscombe, *Polym. J.*, 2017, **49**, 41–60.

8 B. Roth, S. Savagatrup, N. V. de los Santos, O. Hagemann, J. E. Carle, M. Helgesen, F. Livi, E. Bundgaard, R. R. Sondergaard, F. C. Krebs and D. J. Lipomi, *Chem. Mater.*, 2016, **28**, 2363–2373.

9 J. L. Wang, Q. R. Yin, J. S. Miao, Z. Wu, Z. F. Chang, Y. Cao, R. B. Zhang, J. Y. Wang, H. B. Wu and Y. Cao, *Adv. Funct. Mater.*, 2015, **25**, 3514–3523.

10 Y. Z. Lin, Q. He, F. W. Zhao, L. J. Huo, J. Q. Mai, X. H. Lu, C. J. Su, T. F. Li, J. Y. Wang, J. S. Zhu, Y. M. Sun, C. R. Wang and X. W. Zhan, *J. Am. Chem. Soc.*, 2016, **138**, 2973–2976.

11 J. L. Wang, K. K. Liu, J. Yan, Z. Wu, F. Liu, F. Xiao, Z. F. Chang, H. B. Wu, Y. Cao and T. P. Russell, *J. Am. Chem. Soc.*, 2016, **138**, 7687–7697.

12 W. Zhang, J. Smith, S. E. Watkins, R. Gysel, M. McGehee, A. Salleo, J. Kirkpatrick, S. Ashraf, T. Anthopoulos, M. Heeney and I. McCulloch, *J. Am. Chem. Soc.*, 2010, **132**, 11437–11439.

13 H. Bronstein, J. M. Frost, A. Hadipour, Y. Kim, C. B. Nielsen, R. S. Ashraf, B. P. Rand, S. Watkins and I. McCulloch, *Chem. Mater.*, 2013, **25**, 277–285.

14 M. Planells, M. Nikolka, M. Hurhangee, P. S. Tuladhar, A. J. P. White, J. R. Durrant, H. Sirringhaus and I. McCulloch, *J. Mater. Chem. C*, 2014, **2**, 8789–8795.

15 X. Zhang, H. Bronstein, A. J. Kronemeijer, J. Smith, Y. Kim, R. J. Kline, L. J. Richter, T. D. Anthopoulos, H. Sirringhaus, K. Song, M. Heeney, W. Zhang, I. McCulloch and D. M. DeLongchamp, *Nat. Commun.*, 2013, **4**, 2238.

16 D. Venkateshvaran, M. Nikolka, A. Sadhanala, V. Lemaur, M. Zelazny, M. Kepa, M. Hurhangee, A. J. Kronemeijer, V. Pecunia, I. Nasrallah, I. Romanov, K. Broch, I. McCulloch, D. Emin, Y. Olivier, J. Cornil, D. Beljonne and H. Sirringhaus, *Nature*, 2014, **515**, 384–388.

17 Y. J. Cheng, S. H. Yang and C. S. Hsu, *Chem. Rev.*, 2009, **109**, 5868–5923.

18 B. Carsten, F. He, H. J. Son, T. Xu and L. Yu, *Chem. Rev.*, 2011, **111**, 1493–1528.

19 K. Okamoto, J. X. Zhang, J. B. Housekeeper, S. R. Marder and C. K. Luscombe, *Macromolecules*, 2013, **46**, 8059–8078.

20 S.-L. Suraru, J. A. Lee and C. K. Luscombe, *ACS Macro Lett.*, 2016, **5**, 724–729.

21 T. M. McCormick, C. R. Bridges, E. I. Carrera, P. M. Di Carmine, G. L. Gibson, J. Hollinger, L. M. Kozycz and D. S. Seferos, *Macromolecules*, 2013, **46**, 3879–3886.

22 Y. L. Li, T. H. Ren and W. J. Dong, *J. Photochem. Photobiol., A*, 2013, **251**, 1–9.

23 Y. L. Li, Z. P. Li, Y. Wang, A. Compaan, T. H. Ren and W. J. Dong, *Energy Environ. Sci.*, 2013, **6**, 2907–2911.

24 X. Wang, H. Luo, Y. Sun, M. Zhang, X. Li, G. Yu, Y. Liu, Y. Li and H. Wang, *J. Polym. Sci., Part A: Polym. Chem.*, 2012, **50**, 371–377.

25 L. Cai, T. Moehl, S. J. Moon, J. D. Decoppet, R. Humphry-Baker, Z. Xue, L. Bin, S. M. Zakeeruddin and M. Gratzel, *Org. Lett.*, 2014, **16**, 106–109.

26 X. Wang and M. Wang, *Polym. Chem.*, 2014, **5**, 5784–5792.

27 M. Wakioka, S. Ishiki and F. Ozawa, *Macromolecules*, 2015, **48**, 8382–8388.

28 L. Lu and L. Yu, *Adv. Mater.*, 2014, **26**, 4413–4430.

29 W. E. Lee, C. L. Lee, T. Sakaguchi, M. Fujiki and G. Kwak, *Chem. Commun.*, 2011, **47**, 3526–3528.

30 N. Bowden, S. Brittain, A. G. Evans, J. W. Hutchinson and G. M. Whitesides, *Nature*, 1998, **393**, 146–149.

31 C. M. Stafford, C. Harrison, K. L. Beers, A. Karim, E. J. Amis, M. R. VanLandingham, H. C. Kim, W. Volksen, R. D. Miller and E. E. Simonyi, *Nat. Mater.*, 2004, **3**, 545–550.

32 D. Tahk, H. H. Lee and D.-Y. Khang, *Macromolecules*, 2009, **42**, 7079–7083.

33 S. Savagatrup, A. S. Makaram, D. J. Burke and D. J. Lipomi, *Adv. Funct. Mater.*, 2014, **24**, 1169–1181.

34 S. Savagatrup, A. D. Printz, T. F. O'Connor, A. V. Zaretski, D. Rodriquez, E. J. Sawyer, K. M. Rajan, R. I. Acosta, S. E. Root and D. J. Lipomi, *Energy Environ. Sci.*, 2015, **8**, 55–80.

35 K. A. Mazzio, A. H. Rice, M. M. Durban and C. K. Luscombe, *J. Phys. Chem. C*, 2015, **119**, 14911–14918.

36 J. M. Verilhac, R. Pokrop, G. LeBlevennec, I. Kulszewicz-Bajer, K. Buga, M. Zagorska, S. Sadki and A. Pron, *J. Phys. Chem. B*, 2006, **110**, 13305–13309.

37 J. J. Intemann, K. Yao, H.-L. Yip, Y.-X. Xu, Y.-X. Li, P.-W. Liang, F.-Z. Ding, X. Li and A. K.-Y. Jen, *Chem. Mater.*, 2013, **25**, 3188–3195.

38 W. H. Lee and Y. D. Park, *Polymers*, 2014, **6**, 1057–1073.

39 S. Cook, A. Furube and R. Katoh, *Energy Environ. Sci.*, 2008, **1**, 294–299.

40 J. Song, Y. Lee, B. Jin, J. An, H. Park, H. Park, M. Lee and C. Im, *Phys. Chem. Chem. Phys.*, 2016, **18**, 26550–26561.

41 N. I. Nijegorodov and W. S. Downey, *J. Phys. Chem.*, 1994, **98**, 5639–5643.

42 J. R. Lakowicz, *Principles of Fluorescence Spectroscopy*, Springer Science+Business Media, NY, USA, 3rd edn, 2006.

43 W. Hong, B. Sun, H. Aziz, W. T. Park, Y. Y. Noh and Y. Li, *Chem. Commun.*, 2012, **48**, 8413–8415.

44 R. B. Araujo, A. Banerjee, P. Panigrahi, L. Yang, M. Sjodin, M. Stromme, C. M. Araujo and R. Ahuja, *Phys. Chem. Chem. Phys.*, 2017, **19**, 3307–3314.

45 R. Remy, E. D. Weiss, N. A. Nguyen, S. J. Wei, L. M. Campos, T. Kowalewski and M. E. Mackay, *J. Polym. Sci., Part B: Polym. Phys.*, 2014, **52**, 1469–1475.

46 G. J. Hedley, A. J. Ward, A. Alekseev, C. T. Howells, E. R. Martins, L. A. Serrano, G. Cooke, A. Ruseckas and I. D. Samuel, *Nat. Commun.*, 2013, **4**, 2867.